Journal of Marine Research, 68, 413–431, 2010

Rapid response of the East Australian Current to remote wind forcing: The role of barotropic-baroclinic interactions

by K. L. Hill[1,2], S. R. Rintoul[3], P. R. Oke[3] and K. Ridgway[3]

ABSTRACT

The strength of the East Australian Current (EAC) is observed to vary in response to changes in basin-scale winds in the South Pacific, with a time lag of three years. First mode baroclinic Rossby waves would take 10–15 years to reach the western boundary from the center of the South Pacific, so a faster mechanism is needed to explain this link. We use an ocean general circulation model forced with idealized anomalies of wind stress curl to examine the mechanism responsible for the rapid response of the EAC. A curl perturbation in the central South Pacific produces baroclinic and barotropic Rossby waves. The barotropic waves propagate quickly to the western boundary at New Zealand (NZ), where they scatter into a coastal Kelvin wave that travels anti-cyclonically around the coast of NZ. In the Tasman Sea, the height anomaly associated with the Kelvin wave spawns first mode baroclinic waves that take about three years to propagate across the Tasman Sea to influence the EAC. The model suggests that the rapid response of the EAC to changes in wind forcing can be explained by a combination of barotropic and baroclinic Rossby waves with conversion between modes facilitated by topography.

1. Introduction

Subtropical gyres are a dominant feature of the global wind-driven ocean circulation. In the interior of the subtropical basins, geostrophic flow is equatorward. The western boundary current flows poleward, balancing the equatorward transport in the Sverdrup interior and transporting heat from the tropics to higher latitudes. Wind-stress curl determines the strength and spatial pattern of the gyre (Munk, 1950). Hence variations in the basin-scale wind field will drive variability in the strength of the western boundary current. Understanding the dynamics of the relationship between boundary currents and remote wind forcing, and the timescales at which the ocean responds to changes in winds, is essential to explain the cause of observed variations in the western boundary currents at timescales from seasonal to multidecadal.

1. Quantitative PhD Program, University of Tasmania, 7001 Tasmania, Australia.
2. Present address: Integrated Marine Observing System, University of Tasmania, 7001 Tasmania, Australia. ***email: katy.hill@imos.org.au***
3. CAWCR: A Partnership between the Bureau of Meteorology, CSIRO and the Antarctic Climate and Ecosystems CRC, CSIRO Marine and Atmospheric Research, Hobart 7001, Tasmania, Australia.

The East Australian Current (EAC) is the western boundary current of the South Pacific subtropical gyre. The westward flow of the South Equatorial Current (SEC) forms the equatorward limb of the gyre. The SEC reaches the Australian coast between 15°S–22°S and bifurcates, with the southward flow feeding the EAC (Qu and Lindstrom, 2002). Most of the EAC separates from the coast at around 31–34°S to form the Tasman Front (Ridgway and Dunn, 2003; Mulhearn, 1987), which flows across the Tasman Sea and around the northern tip of New Zealand (NZ) to become the East Auckland Current. The remainder of the EAC (the EAC extension) continues south to the east coast of Tasmania, roughly following the shelf edge.

The South Pacific gyre – and hence the EAC – exhibits a long-term strengthening trend related to a strengthening of the subtropical westerly winds in the South Pacific (Cai, 2006; Hill *et al.*, 2008; Ridgway, 2007; Roemmich *et al.*, 2007). The EAC Extension and Tasman Front also have strong decadal variability (Hill *et al.*, 2008, 2011). The strength of the EAC Extension is correlated with changes in wind-stress curl, with transport through the Tasman Sea, and with changes in temperature and salinity at Maria Island off the east coast of Tasmania (42.5°S, 148.2°E) (Hill *et al.*, 2008). The strengthening of the South Pacific gyre and the EAC has been related to stronger westerly winds associated with the Southern Annular mode (Cai, 2006; Roemmich *et al.*, 2007). Decadal variations in the EAC system manifest as an anti-correlation between the strength of the EAC Extension and the Tasman Front (Hill *et al.*, 2011). This variability has been related to decadal ENSO variability via the Pacific South American Mode (Sasaki *et al.*, 2008; Hill *et al.*, 2011).

The East Australian Current (EAC) Extension has been observed to respond to decadal variations in the magnitude of South Pacific wind stress within three years (Hill *et al.*, 2008). However, first mode baroclinic Rossby waves take 10–15 years to cross the Pacific to Australia from the central South Pacific, the region where the wind-stress curl has the highest cross-correlation with the strength of the EAC Extension (Hill *et al.*, 2008). While there are observations of the barotropic response of the ocean in the literature (Vivier *et al.*, 2005; Niiler *et al.*, 1993; Muller and Frankignoul, 1981), recent literature focuses on the baroclincic response of the ocean to wind forcing to explain low frequency variability; Both Qiu and Chen (2006) and Schneider and Miller (2001) concluded that the baroclinic Rossby wave dynamics can explain the observed sea-surface height (SSH) variability in the subtropical gyres of the Pacific on inter-annual to decadal timescales. As Qiu and Chen (2006) force their linear model with basin-scale wind anomalies, it was not possible to isolate the region(s) of forcing that was critical to creating the observed variability in SSH. Qiu and Chen (2006) acknowledged that the model showed less skill in the Tasman Sea, where the high sea level trend seen in the altimeter data is not recreated. Their analysis was also hampered by the length of the satellite altimeter dataset, with only 12 years of data to investigate a decadal signal. Further work by Bowen *et al.* (2006) used altimeter data and a linear model similar to that used by Qiu and Chen (2006) to relate an observed high sea level event north of New Zealand in 1998 to a combination of annual first mode baroclinic Rossby waves and steric heating. The model captures 40–60% of the observed variance between 20–32°S in the southwest and Perkins and Holbrook (2001) suggest that zonal changes in wave speed, Rossby wave reflection from extensive ridges and high Rossby wave modes associated with mean flows are also likely to contribute to the vorticity balance of the region.

Idealized model experiments have been used to explore the influence of topography on the propagation of planetary waves, and the consequences for ocean adjustment. Tanaka and Ikeda (2004) explored variability in the Kuroshio region using a regional model with simple ridge topography and an idealised wind-stress anomaly. They investigated the interaction of barotropic and baroclinic Rossby waves at ocean ridges at different timescales and found that, on seasonal timescales, barotropic wave energy appears to be effectively transmitted to the west of the ridge by conversion to baroclinic modes on the ridge. A simple box model was used by Liu *et al.* (1999a) to explore the Kelvin/Rossby wave dynamics around an island. Liu *et al.* (1999a) suggested that the circulation was set up in three stages: an SSH anomaly was established by baroclinic Rossby waves dissipated against the east coast of the island; the SSH anomaly propagated around the island as a coastal Kelvin wave; and the circulation was completed by long Rossby waves initiated on the west coast of the island.

The work of Tanaka and Ikeda (2004) and Liu *et al.* (1999a) suggests a hypothesis to explain how wind forcing can initiate variability on the western boundary with a lag of a few years. Enhanced wind stress in the central South Pacific generates fast barotropic Rossby waves as well as slow baroclinic waves. On reaching NZ, the barotropic energy is converted to baroclinic energy, and the SSH anomaly propagates anti-cylonically around the coast of NZ as a Kelvin wave. This anomaly spawns baroclinic Rossby waves on the west coast of NZ, which subsequently take a few years to cross the Tasman Sea. Figure 1 summarizes this proposed mechanism.

The aim of our study is to test the idea that interaction between barotropic and baroclinic Rossby waves and topography can explain the observed time lag between changes in the winds and changes in the strength of the East Australia Current. We test this hypothesis by forcing an ocean general circulation model with enhanced winds in a small region and for a limited period, in an attempt to isolate the physical mechanisms responsible for the observed rapid response of the western boundary current to changes in the wind.

2. Model set up

a. *The CSIRO Mk3.5 global ocean model*

We used the CSIRO Mk3.5 global ocean model, which is based on version 4 of the Geophysical Fluid Dynamics Laboratory Modular Ocean Model (MOM4) code (Griffies *et al.*, 2004). The model grid spacing is 1.875° degrees zonally, 0.94° meridionally, and 31 levels in the vertical spaced from 10 m at the surface and 400 m at depth. The model uses Bryan-Lewis vertical diffusivity, which in the tropics ranges from $1 \times 10^{-5}\,\mathrm{m}^2\,\mathrm{s}^{-1}$ at the surface to $1 \times 10^{-4}\,\mathrm{m}^2\,\mathrm{s}^{-1}$ at depth and at high latitudes ranges from $3 \times 10^{-5}\,\mathrm{m}^2\,\mathrm{s}^{-1}$ at the surface to $1 \times 10^{-4}\,\mathrm{m}^2\,\mathrm{s}^{-1}$ at depth (Bryan and Lewis, 1979). Neutral mixing and a

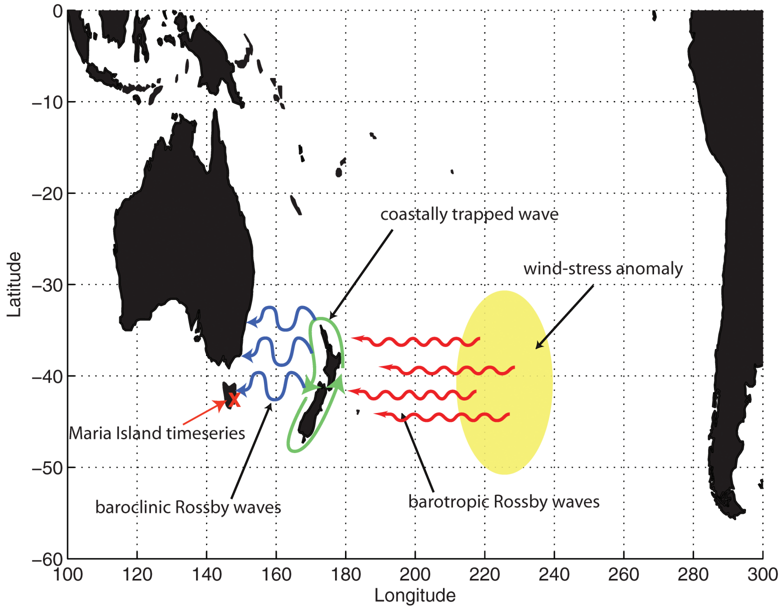

Figure 1. A schematic of the rapid mechanism by which changes in the winds in the South Pacific can be communicated to the East Australia Current.

Laplacian friction coefficient of 3×10^{-4} are used following model tests to ensure friction was kept at a minimum while maintaining model stability. The model restores to climatology (CSIRO Atlas of Regional Seas, CARS) surface temperature (SST) and salinity (SSS) with a timescale of 1 year. The barotropic wave response to the wind stress perturbation does not have any expression on the SST and SSS - so the restoring has no impact there. Similarly, the baroclinic wave does not strongly project onto SST or SSS - so again, the 1 year restoring of SST and SSS to climatology is expected to have minimal impact on the simulated response to the perturbed winds.

Bathymetry is based on Smith and Sandwell (1997). The representation of the bathymetry at model grid spacing is shown in Figure 2. There are about 11 grid cells across the Tasman Sea.

The model is spun up for 200 years with a mean annual cycle calculated from ERA-40 winds. The time-mean ocean streamfunction for the South Pacific (see Figure 3), computed from the 20-year control run, shows a broad scale South Pacific gyre structure with maximum streamfunction values of 50 Sv. This is a sufficiently realistic representation of the gyre to serve as a test bed for a process study exploring the ocean's response to wind-forcing anomalies. Zonal and meridional sections of temperature across the South Pacific were compared with CARS climatology. The stratification in these sections compares well, which is important for simulating topographic interactions realistically (Owen *et al.*, 2005).

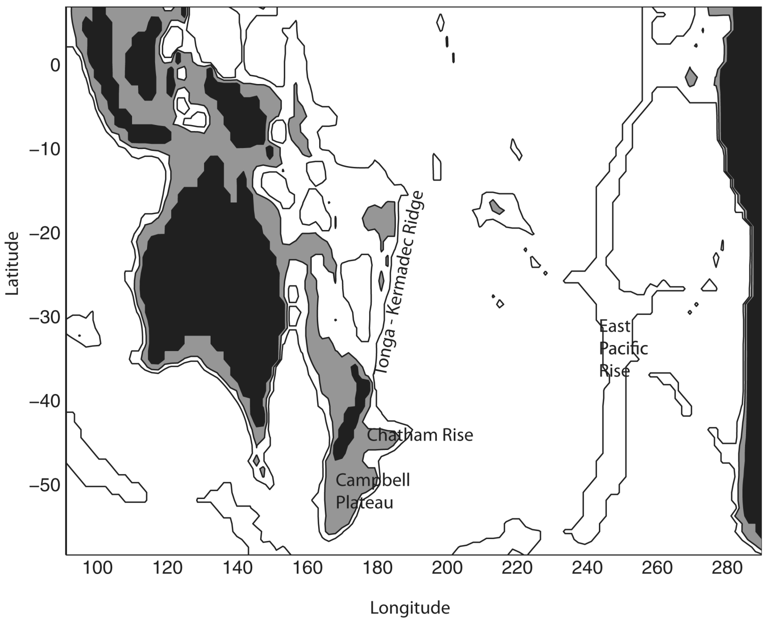

Figure 2. Bathymetry of the South Pacific with major bathymetric features labeled. The black areas are above sea level, grey areas are above 2000 m, and the grey line marks the 3500 m depth contour.

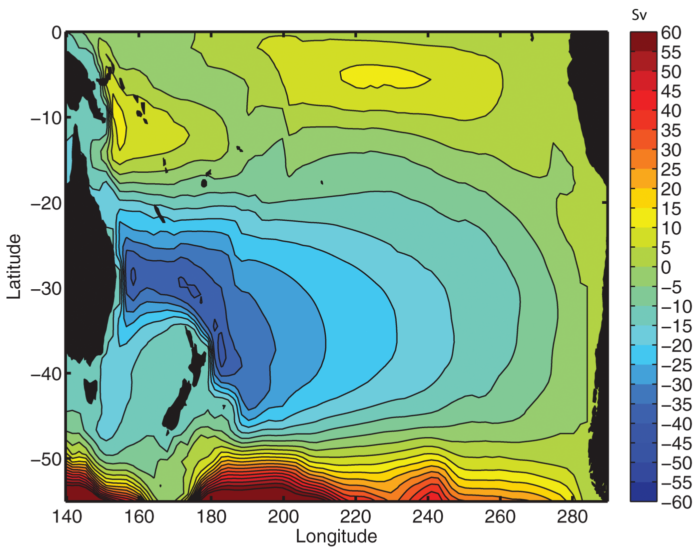

Figure 3. 20-year mean South Pacific streamfunction in Sverdrups (Sv) from the model control run.

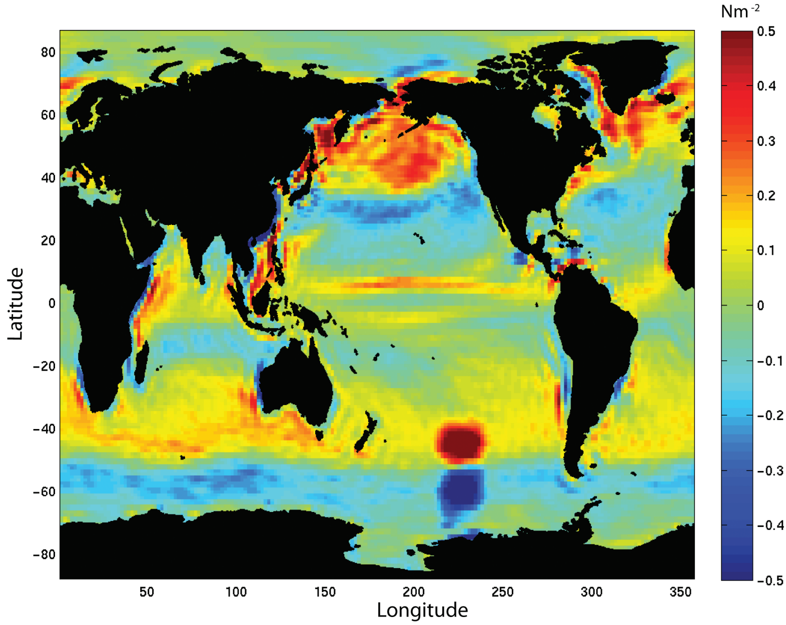

Figure 4. ERA-40 mean January zonal wind stress curl with central perturbation applied (N m^{-2}).

One feature that is not entirely realistic is the transport through the Tasman Sea at 37°S, with a mean value of 3 Sv northward in the model compared to 9.5 Sv southward seen in observations (Ridgway, 2007).

b. Perturbed forcing experiments

The wind-stress curl is modified by adding a zonal wind stress anomaly to the mean seasonal cycle ERA-40 winds over a limited region in the central South Pacific. The anomaly is located to alter the wind stress curl near the maximum curl, where the dominant low frequency variability is observed in reanalysis winds (Hill *et al.*, 2008, 2011). The zonal wind stress is increased by a factor of five in a 10° longitude patch centered on 225°E and then ramps linearly down to observed values over 5° of longitude on either side. In the meridional direction, the wind is linearly increased from observed values at 35°S to five times observed at 50°S and maintained at five times observed to the Antarctic continent. The resulting wind-stress curl pattern used to force the model is shown in Figure 4. The anomaly is applied for 1 year, and then the model is run for a further 19 years.

The magnitude of the anomaly is large to provide a clear signal of the response to the wind forcing (e.g., larger than internal variability in the model) in these idealized experiments. Initial runs where the anomaly was applied for only 1 month did not show a baroclinic response west of NZ. The minimum baroclinic wave period at 45°S is around 300 days,

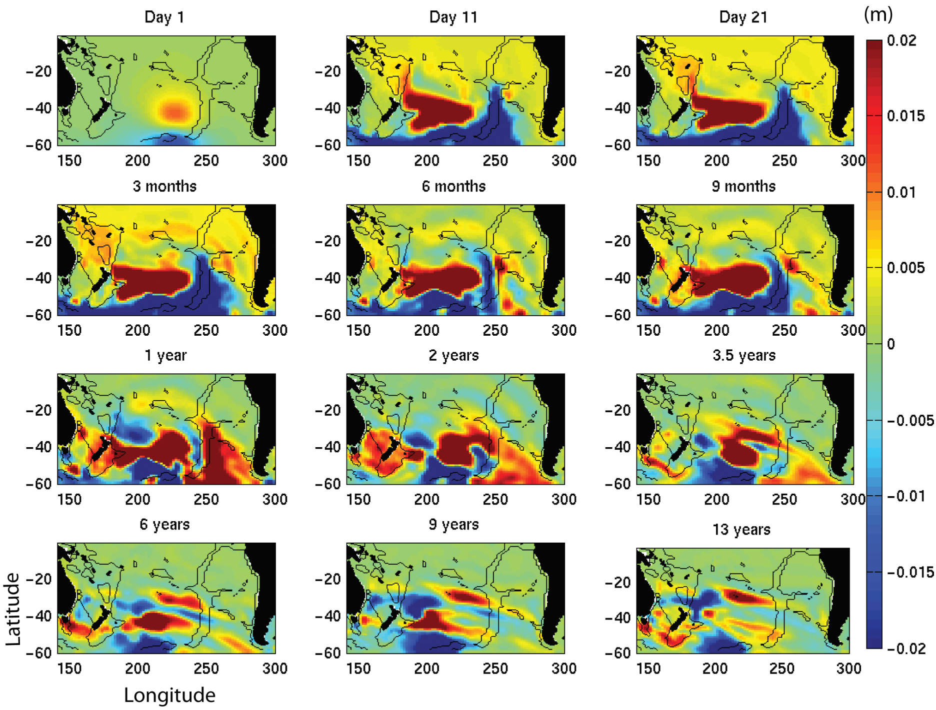

Figure 5. Snapshots of SSH anomaly in meters (forced run – control run) at periods after the initiation of enhanced wind forcing in the central South Pacific. The Black line represents the 3500 m bathymetric contour. Note the uneven time interval between plots.

and over 500 days south of 50°S (Gill, 1982). This may explain why sustained forcing is needed at these latitudes before a discernible response is seen in the Tasman Sea.

3. Results

a. Sea-surface Height (SSH) response

The ocean's response to the enhanced forcing is shown in SSH anomaly fields (Fig. 5). A series of SSH anomaly maps over a period of 13 years gives a picture of how these propagating features evolve, interacting with NZ and the regional topography (see Fig. 2). The 12 maps show the SSH anomaly in the South Pacific at different times after the forcing perturbation.

A SSH anomaly associated with a barotropic wave moves westward rapidly and reaches NZ in week 1. Such a fast propagation is too fast even for barotropic propagation which, travelling at 2 m/s, would take up to 3 weeks to cross to the Tonga-Kermadec Ridge from the central Pacific (Pedlosky, 1996). At a calculated speed of 14 m/s, this feature is likely to be gravity wave propagation (Pond and Pickard, 1983). On reaching the Tonga–Kermadec Ridge to the north of NZ, a 1.2 cm SSH anomaly propagates north along the ridge as a

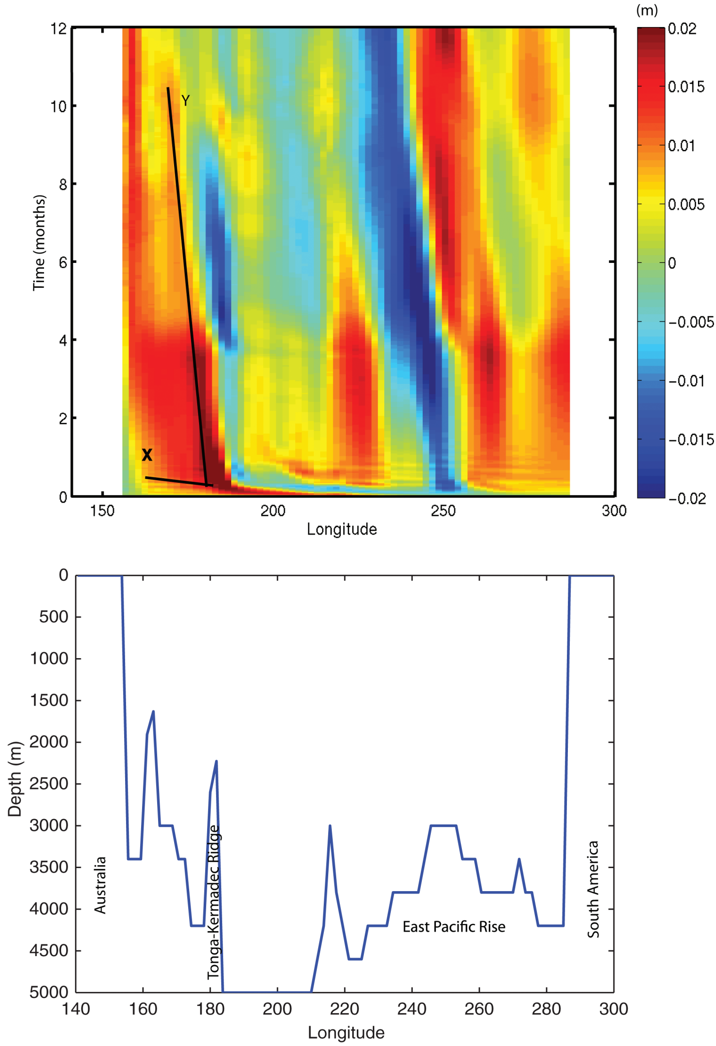

Figure 6. A longitude/time plot of the SSH anomaly in meters (forced run – control run) across 28°S for the first 12 months. Solid lines show the angle at which the speeds of propagating features were calculated.

topographically trapped mode, before scattering westward across the Tasman Sea as a 0.5–1 cm SSH anomaly between 15°S and 30°S, 1 week - 6 months after the beginning of the forcing anomaly. After 6 months, a positive SSH anomaly is seen at 30–32°S off the coast of Australia, which according to the model streamfunction (Fig. 3) is situated in the core of the EAC, close to the separation zone. This propagation pathway can be seen in a Hovm*ü*ller plot along 28°S, and the model's bathymetry profile at this latitude (Fig. 6). It is difficult to

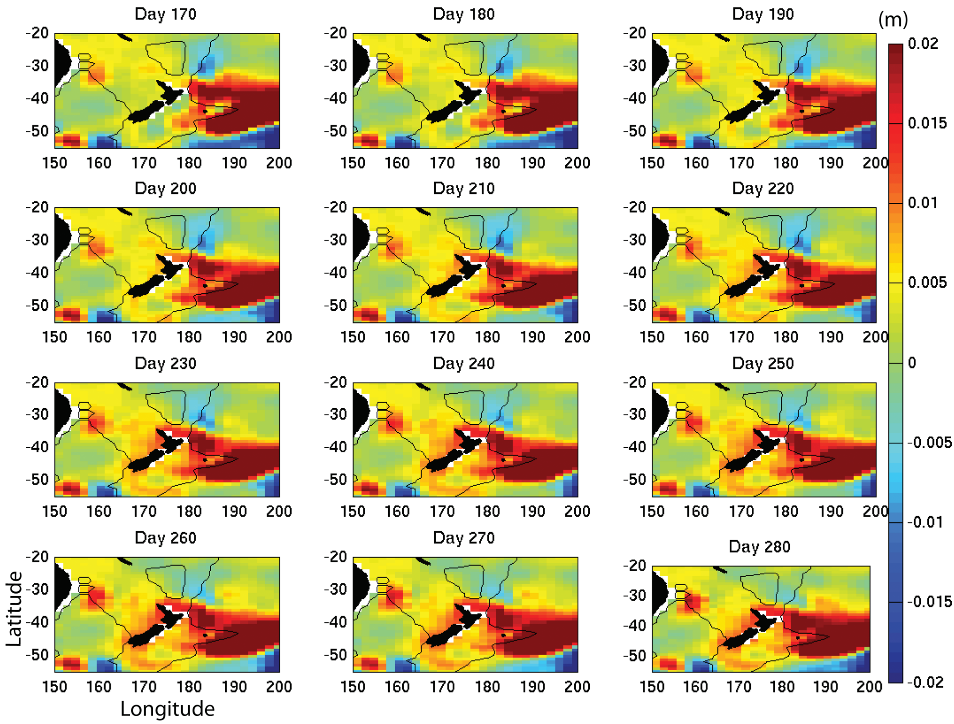

Figure 7. Snapshots of the SSH anomaly in meters (forced run – control run) at periods after the initiation of enhanced wind forcing in the South Pacific. 170 days - 280 days roughly covers the period from 6–9 months.

isolate the speed of propagation, due to the scattering into multiple modes on the ridge. Two lines (marked x and y) are drawn to illustrate the range of speeds. Thus, the speeds calculated from these lines are $X = 1.9\,\mathrm{m/s}$ (close to the expected speed of 2 m/s for a barotropic wave (Pedlosky, 1996)) and $Y = 3.6\,\mathrm{cm/s}$. According to (Killworth *et al.*, 1997), the expected propagation speed at this latitude in the presence of background circulation is 2–4 cm/s, so the feature marked Y is well within this range. This rapid mechanism impacting on the core of the EAC will be the focus of further analysis; this paper focuses on the mechanism driving low frequency variability EAC Extension/Tasman Front.

Farther south, the anomaly stalls at Campbell Plateau and does not cross the shelf for 6 months, when a positive anomaly is seen crossing the shelf toward NZ. A positive anomaly also begins to propagate around to the north of NZ, taking 10 days to propagate around to the west coast of NZ, when a SSH anomaly begins to establish itself along the west coast of NZ. This corresponds to a propagation speed of roughly $1.5\,\mathrm{m\,s^{-1}}$ and is likely to be a coastally trapped (or Kelvin) wave, although the propagation speed is somewhat slower than observed (e.g., $2.7\,\mathrm{m\,s^{-1}}$ (Li and Clarke, 2004)). Figure 7 shows snapshots of the SSH anomaly around NZ at 10-day intervals between day 170 and 280 (about 6–9 months).

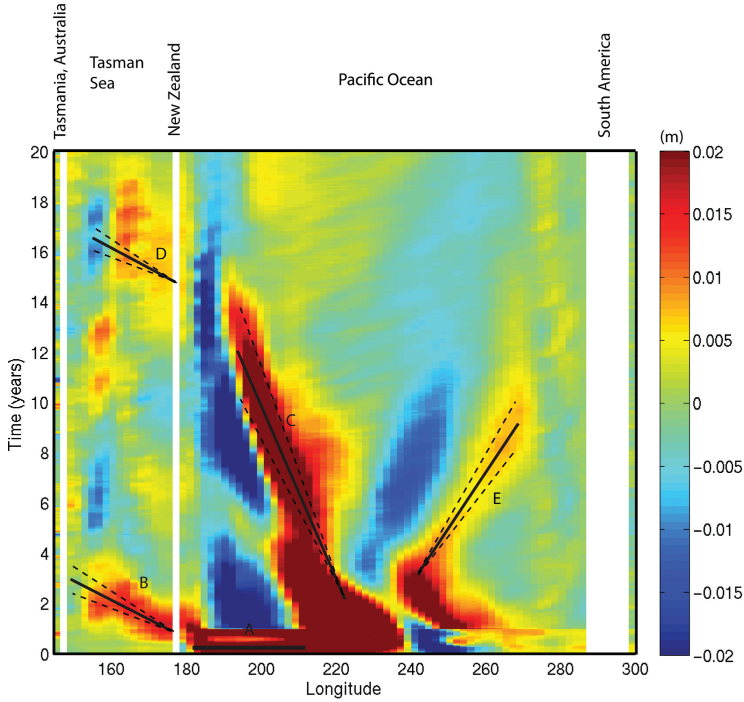

Figure 8. A longitude/time plot of the SSH anomaly in meters (forced run – control run) across 40°S. Solid lines show the angle at which the speeds of propagating features were calculated. Dashed lines represent calculated speeds plus/minus 0.5 cm/s.

An SSH anomaly builds up along the east coast of NZ between 9 months and 1 year. It takes 2–3 years after the initial forcing for the anomaly established along the east coast of NZ to propagate across the Tasman Sea. A second SSH anomaly persists in the South Pacific and propagates slowly westward. This SSH anomaly reaches NZ in 12–14 years.

The rapid initial response to enhanced wind forcing is seen in a Hovm*ü*ller plot across 40°S (feature labeled (A) in Fig. 8). A discontinuity in the plot is apparent after 12 months, which marks the end of the perturbed forcing period. As identified in Figure 5 there is an initial fast westward propagation response which crosses the basin to NZ immediately. While there is some reduction in the size of the SSH signal, an SSH anomaly of 5 cm reaches the east coast of NZ. There is no evidence of barotropic energy produced on the west side of NZ as a result of the coastally trapped wave propagation identified in Figure 5. It takes 8 months for an SSH anomaly to appear on the western side of NZ. The slower propagation of this anomaly can then be seen crossing the Tasman Sea toward Australia (Fig. 8). An SSH anomaly of 2 cm is seen propagating from NZ at around 3.19 cm s^{-1} westwards (labelled B in Fig. 8), reaching the east coast of Australia between 1.5 and 4 years. This is slightly faster than expected from theory; Killworth *et al.* (1997) show that in the presence of a geostrophic flow field (baroclinic U), the range of speeds predicted at 40°S are about 0.5–2 cm/s (95% confidence limits). This combination of barotropic and baroclinic Rossby waves and a coastally trapped wave results in an SSH anomaly reaching the east coast of Australia after 1.5 and 4 years, compared to a time lag observed in observations of 3 years (Hill *et al.*, 2008).

There is a conversion from barotropic to baroclinic wave energy on reaching NZ. A 4 cm SSH response reaches the east coast of NZ and the SSH signal that travels around the north of NZ and reaches the west coast of NZ in the Tasman Sea is 2 cm. This west coast NZ SSH anomaly begins to build up after 6 months. The delay between the barotropic signal hitting the east coast of NZ, and the build up of the SSH anomaly on the west coast appears to be related to the SSH anomaly stalling for 6 months before it is converted from barotropic to baroclinic energy and begins to propagate around the north coast. The propagation of the Kelvin wave also appears to be slightly slower than observations. The slightly slower propagation of the Kelvin wave could be related to the coarse resolution of the model (Hsei *et al.*, 1983).

In addition to the fast response discussed above, a feature that propagates more slowly is spawned directly at the region of forcing in the central Pacific (labeled C in Fig. 8). It has an SSH anomaly of 3 cm and reaches the coast of NZ after 12–14 years (see Fig. 8). This slower feature propagates at 0.7 cm s^{-1}, which is within the range predicted by Killworth *et al.'s* (1997) modified theory for first mode baroclinic waves (0.5-2 cm s^{-1}). This feature also propagates into the Tasman Sea as an SSH anomaly of 0.7 cm.

Speeds, from 0.7 cm/s to 3.2 cm/s have been attributed to baroclinic Rossby waves at 40°S. The lines illustrating $+/-0.5$ cm/s on Figure 8 illustrate the uncertainty our speed estimates could be up to $+/-0.5$ cm/s. The slowest propagation associated with baroclinic wave propagation (the feature labeled C; 0.7 cm/s) is within the theoretical range. The fastest speed associated with a baroclinic wave propagation (labeled (B) in Fig. 8) is 3.19 cm/s is outside the theoretical range, even if an error of $+/-0.5$ cm/s is considered. However, our results are supported by Killworth *et al.* (1997) who acknowledged that the observations still have a bias to faster speeds than predicted; 52% of speeds observed by Chelton and Schlax (1996) lie outside these 95% confidence limits.

An eastward moving feature (labeled E in Fig. 8) is also seen, propagating at about 1.2 cm/s. Comparison of the propagation speed and pathway of this feature in SSH fields (Fig. 5) with the model's streamfunction (Fig. 3) suggests that this SSH anomaly is being advected in the mean field, as opposed to propagating.

b. Variations in transports

Net northward transport through the Tasman Sea for the control run and the forced run are compared in Figure 9 (the more negative the transport, the stronger the EAC Extension). The transports have been smoothed with a 1-year low-pass filter. While some low-frequency variability is apparent in the control run, the magnitude is small (less than 0.5 Sv). Periods

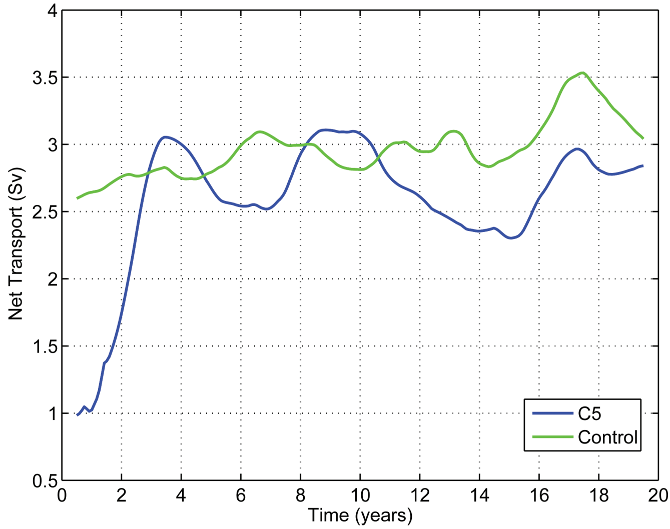

Figure 9. Net northward transport through the Tasman Sea for the control and forced runs (Sv).

of lower net northward transport can be interpreted as periods of strengthened southward transport through the Tasman Sea, and hence a stronger EAC Extension. However, as the SSH anomalies have been calculated by subtracting the control run from the forced run, it is more appropriate to focus on anomalies of transport rather than absolute values (forced minus control run). This isolates the impact of the enhanced forcing from the intrinsic ocean variability.

The transport anomalies for the EAC Extension and Tasman Front are shown in Fig. 10 (positive anomaly = stronger transport of the EAC Extension (south) and Tasman Front (east)), showing that the first peak in the EAC Extension (+2.3 Sv) and trough in the Tasman Front (−2.3 Sv) appears after 6 months (labeled (A) in Fig. 10). If this is compared with Fig. 8, it matches up well with the time that it takes the barotropic response to reach the east coast of NZ, and a topographic wave to travel up the Tonga–Kermadec Ridge, scattering to the west of the ridge (seen after 11 days to 3 months) resulting in an SSH anomaly in the EAC close to the separation zone at 6 months. This scattering and westward propagation could not be attributed to Baroclinic Rossby Waves for certain, as speeds could not accurately be deduced from the hovmuller plots. It may be that the SSH response is confused due to multiple modes. The waves propagate across the Tasman Sea (Fig. 5) over 1–7 months. When baroclinic waves reach the western boundary, they reflect into short-wavelength waves and quickly dissipate, releasing energy into the system and enhancing the transport of the western boundary current (Pedlosky, 1979).

A second minimum in the Tasman Front is seen after 1 year (−4.4 Sv) and the EAC Extension within 1–2 years (1.3 Sv) labeled (B) (Fig. 10). This appears to be associated

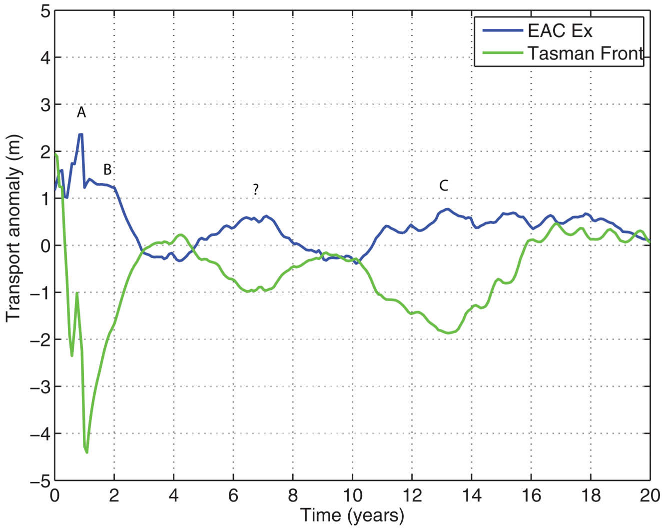

Figure 10. Transport anomaly (forced run – control run) for the EAC Extension and Tasman Front (Sv). Labels associate transport anomalies with propagating features in Figures 6 and 8.

with the build up of the SSH anomaly around the north of NZ propagating as a coastally trapped wave, and the propagation of the positive anomaly across the Tasman Sea (labeled B in Fig. 8), which weakens the Tasman Front and strengthens the EAC Extension. However, some of the signal could be caused by the response of the ocean to the end of the enhanced forcing period. Based on observations (Hill *et al.*, 2008), it would be expected that the response of the EAC Extension would also be stronger. However, as noted in Section 2, the mean net transport through the Tasman Sea is northward, caused by an overly strong return flow of the EAC within the Tasman Sea in the model. The processes governing the separation zone are not resolved at the grid spacing of the model, which may in part explain the weak transport response in the EAC system to a large perturbation in the winds. The dispersive nature of a coarse model such as this may also have an effect.

After 6–8 years, a third minimum in the Tasman front (−1 Sv) and peak in the EAC Extension (0.5 Sv) are seen (labeled (?)), there is a region of high sea level in the southern Tasman Sea at the same time (Fig. 5), but analysis of sea level patterns could not associate this sea level anomaly with a propagating feature. After 12–14 years, a fourth minimum in the Tasman Front (−1.8 Sv) and a peak in the EAC Extension (0.7 Sv) are seen (labeled C in Fig. 10). The Tasman Front minimum is related to the first mode baroclinic Rossby wave reaching NZ and causing an increase of SSH around the north of NZ, hence weakening the Tasman Front. This suggests a direct negative (or damping) affect of this anomaly on the strength of the Tasman Front. In terms of mass balance, if the water does not exit the Tasman Sea via the Tasman Front, then it must continue south. Hence a reduction in the strength of the Tasman Front would enhance the strength of the EAC Extension. There is not a clear

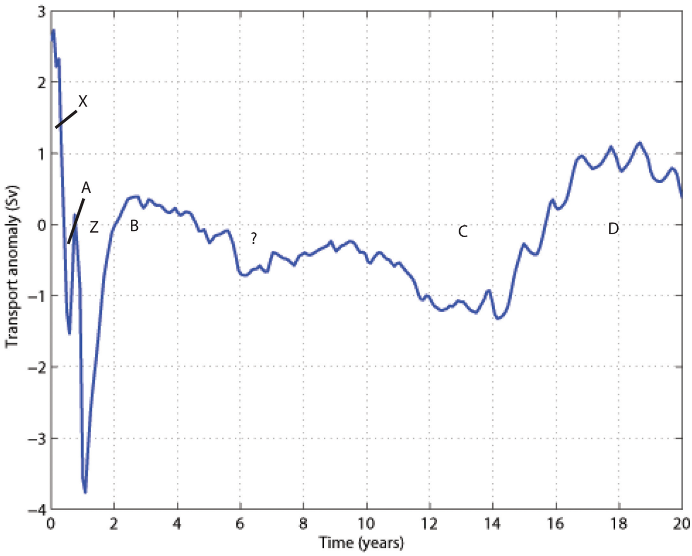

Figure 11. Total EAC Transport anomaly: EAC Extension + Tasman Front (Sv). Labels associate transport anomalies with propagating features in Figures 6 and 8.

impact on the strength of the EAC Extension; the small anomaly in the EAC Extension is a similar magnitude to variability seen in the control run. Interestingly, with a single isolated pulse of perturbation to the winds, the model produces low frequency variability in the strength of the EAC Extension and Tasman Front. The strength of these two currents are also anti-correlated ($r = -0.54$), as observed Hill *et al.* (2011).

EAC total transport anomaly was calculated by summing the EAC Extension and the Tasman Front transport (Fig. 11). As the model has very week net southward flow through the Tasman Sea, this may give a different picture of the response of the EAC to single pulse forcing. There is an immediate positive response of 2.5 Sv during the first 3–4 months (labeled (X) on Fig. 11), which matches the timing of the scattering of energy across the Tasman Sea from the Tonga-Kermadec Ridge (also labeled (X) in Figure 6. This is followed by a sharp negative response at 6 months of −1.5 Sv (labeled (A) in Fig. 11), which matches the timing of when the initial barotropic response (labeled (A) in Fig. 8) crosses the shelf to the east of New Zealand, and begins to propagate around New Zealand; another sharp negative response at just after 1 year, of about −3.7 Sv is seen (labeled (Z) in Fig. 11). It is not clear what causes this, but it may be due to the adjustment of the model to the end of the enhanced forcing period. There are two further negative responses; one of −0.7 Sv at around 6 years (labeled (?) in Fig. 11) and −1.2 between 12 and 14 years (labeled (C) in Fig. 11). As with the discussion above it is not clear what is causing feature (?) (see Figs. 8 and 5). Feature (C) can be associated with propagating feature (C) in Figure 8, which reaches New Zealand in 12–14 years. The build up of SSH along the northern coast of New

Zealand acts to weaken the Tasman Front. However, due to the strong recirculation in the Tasman Sea, this is unlikely to be translated into a strengthened EAC Extension, causing a net weakening of the EAC. There are two weaker positive responses, peaking at 2–3 years, 0.4 Sv (labeled (B) in Fig. 11) and 18 years, 1.1 Sv (labeled (D) in Fig. 11). These two peaks line up well with when the two baroclinic propagating features cross the Tasman Sea (also labeled (B) and (D) respectively in Fig. 8). This also suggests that these model experiments can achieve a response approaching the 3-year lag seen in the observations (Hill *et al.*, 2008); however, the strong recirculation in the Tasman Sea means that this is not translated into a net increase in transport through the Tasman Sea as the EAC Extension.

4. Discussion

A global ocean model forced with idealized wind-forcing anomalies is used to show that barotropic waves, interacting with topography to produce baroclinic waves, could influence the timescales of variability and response in the subtropical ocean. Specifically, the model results demonstrate a mechanism that can explain the observed 3-year lag between changes in the South Pacific winds and changes in the EAC (Hill *et al.*, 2008). The mechanism is summarized in Figure 1. Barotropic waves propagate west across the Pacific, interacting with the east coast of NZ to scatter into a coastally trapped wave which propagates anti-cyclonically around the island, spawning baroclinic waves that cross the Tasman Sea, giving a total transit time of about 3 years.

The model results also show how Rossby waves interact with deep bathymetry and indicate that the processes discussed by Tanaka and Ikeda (2004) in the North Pacific context are also relevant to the South Pacific. In our model, the barotropic waves reach the Tonga–Kermadec Ridge to the north of NZ, then propagate north as a topographic wave. It appears to build up along the ridge before spilling over to propagate across to the east coast of Australia, similar to some of their experiments. Tanaka and Ikeda (2004) concluded that the balance between barotropic and baroclinic modes was related to the period of forcing. However, experiments with forcing of different periods were beyond the scope of this study.

Previous studies have focused on the contribution of first mode baroclinic waves in attempts to explain the response of the ocean to changes in wind forcing (Qiu and Chen, 2006; Bowen *et al.*, 2006; Sasaki *et al.*, 2008). However, Qiu and Chen's (2006) model showed a sea level trend that is farther south and east than observed (and, in fact, similar in pattern to the wind forcing, as expected given the slow propagation of first mode baroclinic waves at these latitudes). The observed SSH variability in the Tasman Sea is also not reproduced. Sasaki *et al.* (2008) suggest that the results of Qiu and Chen (2006) would be improved if the role of NZ was taken into account, referring to the mechanism put forward by Liu *et al.* (1999a). A comparison between our results and those of Qiu and Chen (2006), Bowen *et al.* (2006) and Sasaki *et al.* (2008) can be considered in the context of the differences in experiment set up. Qiu and Chen (2006) and Sasaki *et al.* (2008) compare results with altimeter data at 7-day intervals whereas barotropic waves have only been detected in 3-day interval data (Fu, 2004). Variability in the southern hemisphere westerlies is generally zonally coherent (Hill *et al.*, 2011) associated with the waxing and waning of the polar vortex and Rossby waves integrate the wind forcing along their path. If the forcing region is just east of NZ, first mode baroclinic waves could explain the observed response. If the the critical region of forcing is farther east, as shown in Hill *et al.* (2008), then a faster (barotropic/baroclinic) mechanism is required.

There is a pause of 6 months before the build up of SSH east of NZ begins to propagate around to the north of NZ as a coastally trapped wave. Tanaka and Ikeda (2004) also see a stalling of wave propagation on ridges, but for a period of around 4 years; in both cases, it is not clear what dynamics are associated with this stalling. The model presented here is forced with realistic winds that are then enhanced by $5\times$ background wind forcing in an isolated region; whereas Tanaka and Ikeda (2004) used a model at rest and forced it with realistic wind stress in an isolated region. This means that in the region of forcing, the model was being perturbed by winds which were around 5 times larger than in the experiments performed by Tanaka and Ikeda (2004). If a critical level of build up is needed before Rossby waves can cross the ridge, this would be reached quicker with the larger perturbations used in this study. The baroclinic wave period of 100 days at 20°S and 300+ days at 45°S may also have an impact on the delay in conversion of barotropic to baroclinic energy (Gill, 1982). This could also account for the observed lag of a few months between when barotropic waves reach NZ, and baroclinic waves are initiated.

Our model results corroborate the conclusions of Hill *et al.* (2011) that the observed anti-correlation between the EAC Extension and the Tasman Front on decadal timescales may be related to variations in the magnitude of the South Pacific wind-stress curl maximum, whereby periods of enhanced wind-stress curl cause the EAC Extension to be favored over the Tasman Front. A small transport response in the EAC Extension and Tasman Front at 1–2 years after the wind perturbation was produced, which related to the barotropic/baroclinic propagation pathway seen in SSH. A slightly clearer response is seen in the total EAC transport (EAC Extension + Tasman Front) centered on 3 years (1.5–4 years). Considering the wind forcing is $5\times$ background wind forcing, the transport response in the Tasman Sea currents was relatively small ($0.5 - 1.5$ Sv). Observed decadal variability in the EAC Extension transport from XBT data is 6–12 Sv (Hill *et al.*, 2011) as a result of wind-stress curl variability in the South Pacific of $4 - 6 \times 10^{-8}\ \mathrm{N/m^2}$ from NCEP (equivilent to a $1.5\times$ increase). The weaker than expected transport anomalies could be related to several factors. The response of this coarse-resolution model is damped by the relatively large dissipation and friction coefficients needed to make the model numerically stable. In addition, the grid spacing of the model means that the nonlinear processes that govern the western boundary current system and its separation from the coast are not resolved, so the EAC Extension is weaker and the Tasman Front is stronger compared to observations. Hill *et al.* (2011) noted that the coarser the resolution of the model, the stronger the Tasman Front is compared to the Tasman Sea. In our model runs, the net transport through the Tasman Sea is northward rather than southward which may result in the modeled EAC responding differently. The limited extent of the imposed wind anomaly could also be a factor. In the real ocean, Rossby waves act as integrators of ocean forcing, and are forced as they travel across an ocean basin, which would offset the dissipation of energy.

We were not able to determine the efficiency of the energy conversion from the barotropic to baroclinic mode. From the model output, it is difficult to isolate the energy of the different wave modes produced by the anomalous forcing from the energy of the background state. More importantly, we do not expect the energy conversion to be very efficient. Most of the incoming energy would be expected to be reflected in short Rossby waves that are rapidly damped to the east of the western boundary (Pedlosky, 1965). Liu *et al.* (1999b) provide further discussion of this point and the importance of distinguishing between the mass and energy budgets. They conclude that much of the incoming energy is dissipated by the short Rossby waves, while the mass transport is largely balanced by the Kelvin wave and long Rossby wave generated at the western side of the island.

By forcing the ocean with a wind anomaly localized in space as well as time, as opposed to observed wind variability, these model experiments help to elucidate the mechanisms by which the ocean responds to changes in wind forcing. The experiments demonstrate, for the first time, the feasibility of a fast combined barotropic–baroclinic mechanism causing a change in the transport of the EAC system on observed timescales. The observed anti-correlation between the EAC Extension and the Tasman Front can also be created by enhancing the maximum wind stress curl. However, the limitations of this study are largely related to the resolution of the model which meant that the propagation of Rossby waves across the Tasman Sea were not necessarily translated into a enhanced southward transport in the EAC Extension; and a combination of the resolution and the localized wind anomaly meant an unrealistically large magnitude wind anomaly required to form a clear response in the ocean. Further work could be done utilizing a higher resolution eddy resolving model to ensure that the processes at the separation point, and hence transport of the EAC Extension and Tasman Front, were more realistic. It could also be used to see if the coastally trapped wave propagation characteristics were closer to observed speeds. Lastly, a higher resolution, and hence less diffuse model, with a more realistic (stronger) EAC Extension would mean that more realistic increases in wind stress could be explored.

Acknowledgments. The authors would like to thank Paolo Cipolini, Jeff Blundell and three anonymous reviewers for their thoughtful comments, and Russ Fiedler for modeling support. This work was conducted as part of the Quantitative Marine Sciences PhD Program, a joint initiative between the University of Tasmania and CSIRO. This study was supported in part by the Department of Climate Change and Energy Efficiency through the Australian Climate Change Science Program and the Australian Government Cooperative Research Centre (CRC) program through the Antarctic Climate and Ecosystems CRC.

REFERENCES

Bowen, M., P. Sutton, and D. Roemmich. 2006. Wind-driven and steric fluctuations of sea surface height in the southwest Pacific. Geophys. Res. Lett., *33*, doi: 10.1029/2006GL026160.

Bryan, K. and L. J. Lewis. 1979. A water mass model of the World Ocean. J. Geophys. Res., *84*, 2503–2517.

Cai, W. 2006. Antarctic ozone depletion causes an intensification of the Southern Ocean super-gyre circulation. Geophys. Res. Lett., *33*, L03712.

Chelton, D. and M. Schlax. 1996. Global observations of oceanic rossby waves. Science, *272*, 234–238.

Fu, L. 2004. Latitudinal and frequency characteristics of westward propagation of large-scale oceanic variability. J.Phys. Oceanogr., *34*, 1907–1921.

Gill, A. E. 1982. Atmosphere-Ocean Dynamics, Academic Press, NY, 662 pp.

Griffies, S., R. Pacanowski, and A. Rosati. 2004. A technical guide to MOM4. GFDL Ocean Group Technical Report 5, NOAA/Geophysical Fluid Dynamics Laboratory.

Hill, K. L., S. R. Rintoul, R. Coleman, and K. R. Ridgway. 2008. Wind forced low frequency variability in The East Australian Current. Geophys. Res. Lett., *35*, doi: 10.1029/2007GL03912.

Hill, K. L., S. R. Rintoul, K. R. Ridgway, and P. R. Oke. 2011. Decadal changes in the South Pacific western boundary current system revealed in observations and reanalysis state estimates. J. Geophys. Res. (in press).

Hsei, W., M. Davey, and R. Wajsowicz. 1983. The free Kelvin wave in finite-difference numerical models. J. Phys. Oceanogr., *13*, 1383–1397.

Killworth, P., D. Chelton, and R. DeSzoeke. 1997. The speed of observed and theoretical long extra-tropical planetary waves. J. Phys. Oceanogr., *27*, 1946–1966.

Li, J. and A. Clarke. 2004. Coastline direction, interannual flow and the strong El Niño currents along Australia's nearly zonal southern coast. J. Phys. Oceanogr., *34*, 2373–2381.

Liu, Z., L. Wu, and H. Hurbert. 1999a. Rossby wave - coastal Kelvin wave interaction in the extratropics. Part II: Formation of island circulation. J. Phys. Oceanogr., *29*, 2405–2418.

—— 1999b. Rossby wave-coastal Kelvin wave interaction in the extratropics. Part I: Low frequency adjustment in a closed basin. J. Phys. Oceanogr., *29*, 2382–2404.

Mulhearn, P. 1987. The Tasman Front - A study using satellite infrared imagery. J. Phys. Oceanogr., *17*, 1148–1155.

Muller, P. and C. Frankignoul. 1981. Direct atmospheric forcing of geostrophic eddies. J. Phys. Oceanogr., *11*, 287–308.

Munk, W. H. 1950. On the wind-driven ocean circulation. J. Meteor., *7*, 79–93.

Niiler, P., J. Filloux, W. Liu, R. Samelson, J. Paduan, and C. Paulson. 1993. Wind-forced variability of the deep eastern North Pacific: Observations of seafloor pressure and abyssal currents. J. Geophys. Res., *98*, 22589–22602.

Owen, G., A. Wilmot, I. Abrahams, and H. Mansley. 2005. The scattering of Rossby waves from finite abrupt topography. Geophys. Astrophys. Fluid Dyn., *99*, 219–239.

Pedlosky, J. 1965. A note on the western intensification of the oceanic circulation. J. Mar. Res., *23*, 207–209.

—— 1979. Geophysical Fluid Dynamics, Springer-Verlag, NY, 689 pp.

—— 1996. Ocean Circulation Theory, Springer, NY, 435 pp.

Perkins, M. and N. Holbrook. 2001. Can Pacific Ocean thermocline depth anomalies be simulated by a simple linear vorticity model? J. Phys. Oceanogr., *31*, 1786–1806.

Pond, S. and G. L. Pickard. 1983. Introductory Dynamical Oceanography, 2nd ed., Butterworth-Heinemann, Jordon Hill, Oxford, 329 pp.

Qiu, B. and S. Chen. 2006. Decadal variability in the large-scale sea surface height field of the South Pacific Ocean: Observations and causes. J. Phys. Oceanogr., *36*, 1751–1762.

Qu, T. and E. J. Lindstrom. 2002. A climatological interpretation of the circulation in the western South Pacific. J. Phys. Oceanogr., *32*, 2492–2508.

Ridgway, K. R. 2007. Long term trend and decadal variability of the southward penetration of the East Australia Current. Geophys. Res. Lett., *34*, L13613, doi: 10.129/2007GL030393.

Ridgway, K. R. and J. R. Dunn. 2003. Mesoscale structure of the East Australian Current system and its relationship with topography. Prog. Oceanogr., *56*, 189–222.

Roemmich, D., J. Gilson, R. Davies, P. Sutton, S. Wijffels, and S. Riser. 2007. Decadal spin up of the deep subtropical gyre in the South Pacific. J. Phys. Oceanogr., *37*, 162–173.

Sasaki, Y., S. Minobe, T. Kagimoto, M. Nonaka, and H. Sasaki. 2008. Decadal sea level variability in the South Pacific in a global eddy resolving model. J. Phys. Oceanogr., *38*, 1731–1747.

Schneider, N. and A. J. Miller. 2001. Predicting western North Pacific climate. J. Clim., *14*, 2997–4002.

Smith, W. H. F. and D. T. Sandwell. 1997. Global seafloor topography from satellite altimetry and ship depth soundings. Science, *277*, 1957–1962.

Tanaka, K. and M. Ikeda. 2004. Propagation of Rossby waves over ridges excited by interannual wind forcing in a western North Pacific mode. J. Oceanogr., *60*, 329–340.

Vivier, F., K. Kelly, and M. Harismendy. 2005. Causes of large-scale sea level variations in the Southern Ocean: Analyses of sea level and a barotropic model. J. Geophys. Res., *110*, C09014.

Received: *25 March, 2010*; revised: *20 December, 2010*.